Materials and methods

Animals, parasites and preparation of materials

The Japanese strain of *S. japonicum* has been maintained in our laboratory for 25 years by passage through *Oncomelania hupensis nosophora* and rabbits. C57BL/6 female mice were purchased from the Shizuoka Laboratory Animal Center (SLC), Japan.

Fresh cercariae emerging from infected snails were fixed in 4% paraformaldehyde in 0.13 M phosphate buffer. Some were processed for whole mount preparations; they were placed on slides coated with poly-L-lysine and fixed again in paraformaldehyde. The other fixed cercariae were implanted into mouse livers through the cecal vein to investigate the details of the TGF-beta-immunoreactive structure. The liver was removed and fixed in the same fixative 30 min later. To investigate the skin migrating stage of schistosomula, mice were percutaneously exposed to 100 cercariae on the shaved abdomen by the ring method. Mice were killed 0.5, 8, 24, and 48 h later. The exposed site was removed and fixed in the paraformaldehyde solution. Livers containing deposited eggs and adult worms were collected from mice infected for 7 weeks and fixed with the same fixative. Paraformaldehyde fixed specimens were routinely processed and embedded in paraffin wax, and sections (4–10 μm thickness) were cut.

For western blot analysis, cercariae were pelleted by centrifugation, sonicated and ground using polytron (Kinematica, Switzerland). The preparation of egg and adult worm extracts was described previously (Hirata et al. 1997). To collect eggs, infected mouse livers and intestines were digested with pronase and collagenase and filtered through several meshes. Eggs were washed with phosphate-buffered saline (PBS) six times by light centrifugation (600 rpm, 2 min).

Immunohistochemistry

For immunoenzyme staining, the sections and whole-mount preparations were preincubated with Block Ace (Yukijirushi, Japan) for 1 h at room temperature (RT) followed by either rabbit anti-mouse TGF-β_1, -β_2 or -β_3 antibody (raised against C-terminal peptide, Santa Cruz, Santa Cruz, Calif)(1:100) or normal rabbit IgG, as a control, overnight. They were incubated with biotinylated anti-rabbit IgG (1:200) (Vector Laboratories, Burlingame, Calif.) for 1 h and endogenous peroxidase activity was blocked with methanol containing 10% H_2O_2. After incubation with the avidin-biotin-peroxidase complex (Vector) for 50 min, reactions were developed with 3-amino-9-ethylcarbazole. The slides were counterstained with Meyer's hematoxylin.

The fluorescent immunohistochemical procedure was as described previously (Hirata et al. 2000, 2003). Briefly, the sections and whole-mount preparations were incubated with antibody to TGF-β_1, -β_2 or -β_3 diluted 1:100 in PBS overnight at RT, and then with FITC-conjugated horse anti-rabbit IgG (Vector) for 4 h at RT. To identify the cell nuclei, the sections and whole-mount preparations were counterstained with propidium iodide (PI) by using Vectashield mounting medium with PI (Vector).

Controls were processed identically and in parallel, however, they were incubated with non-immune rabbit IgG (1:100) rather than with primary antibodies. In the peptide blocking test, primary antibodies were mixed with each corresponding blocking peptide of TGF-β_1, -β_2 or -β_3 (Santa Cruz) at a 1:2 or 1:4 molar ratio and incubated overnight at 4°C and staining was performed as above. In some experiments, antibodies were mixed with an unrelated peptide (anti-TGF-β_3 plus TGF-β_1 blocking peptide) to confirm the specificity.

Confocal laser scanning microscopy

The sections and whole mount preparations double-labeled with FITC and PI were scanned using excitation at 488 nm (argon laser) for FITC and at 568 nm (krypton laser) for PI with a confocal laser scanning imaging system (LSM-GB200 or LSM-FV300, Olympus, Japan). Optical sections of the Z-series of each fluorescence (at consecutive focal levels of 1 μm) were separately taken on channel 1 and channel 2 to avoid any cross-talk and then superimposed. For whole-mount cercariae, the images of both fluorescences were further overlaid with differential interference contrast (DIC) images by LSM-FV300. For analyzing the entire features of cercariae, the images of the Z-series were examined side by side and added to reconstruct a single two-dimensional image. The images were taken using a 10×, 20× or 40× objective lens.

Western blot analysis

The protein concentration of schistosome extracts was determined by Micro BCA protein assay (Pierce, Rockford, Ill.). The extracts were dissolved in reducing sample buffer containing 50 mM Tris-HCl (pH 6.8), 2% SDS, 0.6% 2-mercaptoethanol, 10% glycerin and 0.03% bromophenol blue, and analyzed using 12.5% polyacrylamide gels in the presence of SDS (Laemmli 1970). Proteins were transferred onto PVDF membrane. The membrane was blocked with 100% Block Ace at 4°C for 16 h and then immunoenzymatically labeled using anti-TGF-β_1, -β_2 or -β_3 antibody (1:1000) and peroxidase-conjugated goat anti-rabbit IgG (1:10,000) (Vector). The reaction was developed by SuperSignal West Pico Chemiluminescent substrate (Pierce).

Results

Immunoreactivity in skin stage

Immunoenzyme staining of cercariae-exposed mouse skin (0.5 h) revealed immunoreactivity for all TGF-β isoforms, TGF-β_1, -β_2 and -β_3, in the body of schistosomula, i.e. at the surface and inside the body (Fig. 1a–c). In control studies, no specific reactivity was seen when the primary antibody was substituted with normal rabbit IgG. In the peptide blocking study, no reactivity was seen (a representative experiment is shown in Fig. 1d), and parallel control experiments that used unrelated peptides did not affect the reactivity. Thus, the expression of TGF-β-like molecules in parasites was considered to be specific. Similar experiments were performed on the fluorescence-labeled specimens (below) and confirmed the specificity.

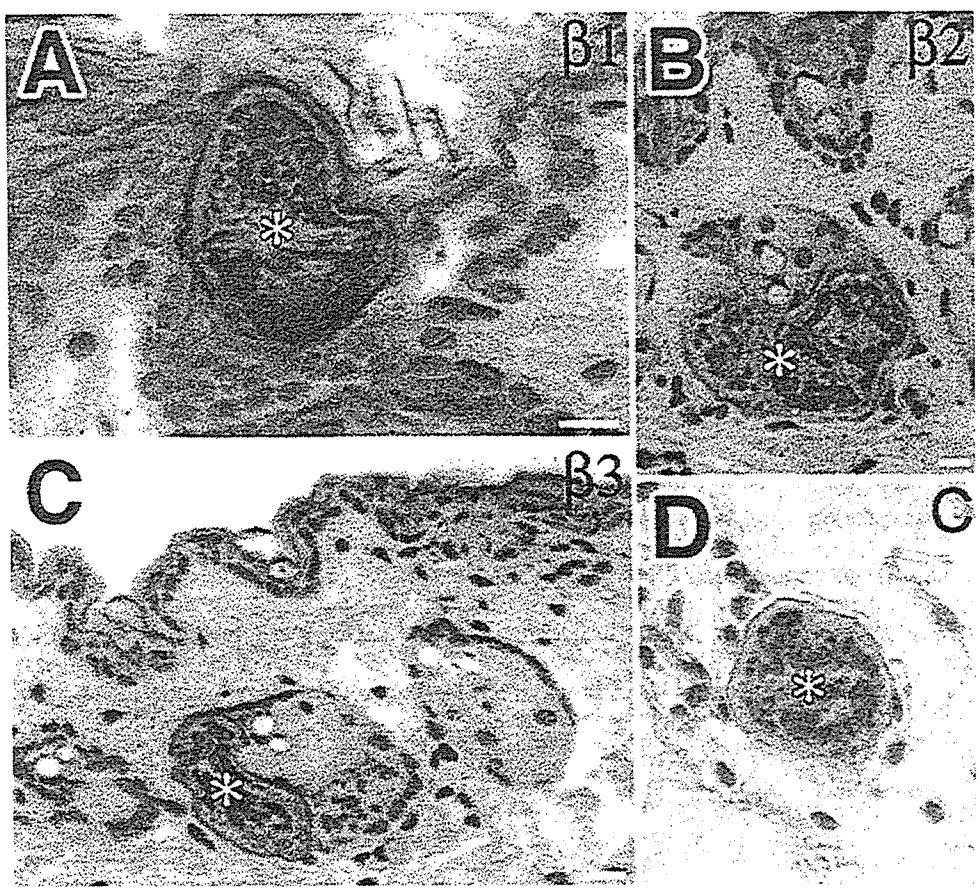

Fig. 1 Expression of TGF-β isoforms in 0.5-h schistosomula of *Schistosoma japonicum*. **a** Immunoenzyme staining of TGF-β_1, **b** TGF-β_2, and **C** TGF-β_3 is shown. Strong immunoreactivity for each TGF-β isoform was localized at the surface of schistosomulum (*asterisks*). Note that weak immunoreactivity for TGF-β_2 (**b**) and TGF-β_3 (**c**) was seen in the epidermis of mouse skin. **d** In a blocking test for TGF-β_3, no immunoreactivity was evident at the surface of schistosomula (*asterisk*). *Bar* 10 μm

Localization of TGF-β isoforms in cercariae

We investigated the detailed localization of each immunoreactive TGF-β isoform using cercariae that were previously paraformaldehyde-fixed and implanted into the mouse liver. Confocal laser scanning microscopy (CLSM) showed specific localization of all TGF-β isoforms in the tegument and the presence of cells expressing TGF-β-like molecules in the subtegumental area (Fig. 2a–c). The number and distribution of producing cells or cellular localization of immunoreactive molecules differed significantly with each isoform. For TGF-β_1, only a few immunoreactive cells were found in the subtegumental area (Fig. 2A), and its expression appeared to be limited to only a part of the cytoplasm, while the parasite tegument was intensely stained. Another characteristic finding for TGF-β_1 was strong reactivity at one region of the parasite surface. The Z-series of CLSM images on the whole parasite body revealed that this region had a pot-like structure (Fig. 2d). Comparison with serial sections, hematoxylin-eosin (H-E) stained preparations and with the previously described diagram of cercariae (Takahashi 1928), showed this region to be the ventral sucker.

TGF-β_2-immunoreactive elements were distributed diffusely over the body (Fig. 2b). In addition, the immunoreactivity at the tegument was rather weak compared with that for TGF-β_1 or TGF-β_3. TGF-β_3-immunoreactive cells were more numerous and stronger in intensity at the subtegumental area in comparison with TGF-β_1 and TGF-β_2 (Fig. 2c). Furthermore, in some TGF-β_3-immunoreactive cells, cytoplasmic processes (arrows) appeared to be continuous with the tegument, suggesting the molecules were being carried to the surface. In order to determine whether TGF-β-like molecules are mouse host-driven or not, whole mount preparations of free-living cercariae were analyzed by both CLSM and DIC after fluorescent immunohistochemical staining. The immunoreactivity was consistently recognized on the whole surface of the cercarial body, suggesting that the molecules are not derived from mouse host (Fig. 2e).

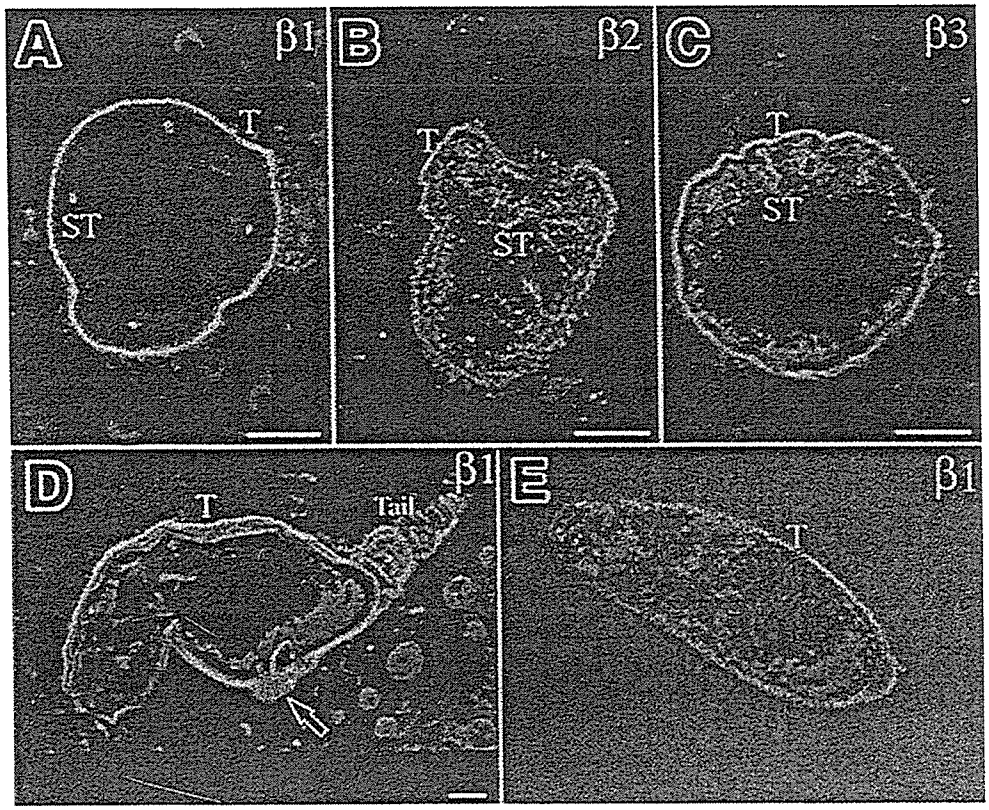

delete

Fig. 2 Detail of the localization of TGF-β isoforms in *S. japonicum* cercariae, which were embedded into the mouse liver (**a–d**) and was prepared in free-living condition (**e**). **a–c** Distribution of TGF-β_1, β_2 and β_3, respectively, in transverse sections of cercaria. ~~*Arrows* in **c** show cytoplasmic processes.~~ **d** TGF-β_1 in a longitudinally-sectioned cercaria. Three images of the Z-series with a distance of 3 μm were overlaid. Note the intensely stained pot-like structure (*arrow* in **d**), which was regarded as the ventral sucker. *Bar* 10 μm. **e** Localization of TGF-β_1 in the surface of a cercaria in a whole-mount preparation. Fluorescent immunoreactivity for TGF-β_1 is shown as *green* (FITC), whereas nuclei are *red* (PI). *Bar* 50 μm. *T* Tegument, *ST* subtegumental cell

Changes in immunoreactivity in the skin migrating stage

When TGF-β expression was examined at 8, 24 and 48 h after cercarial exposure to the skin, immunohistochemical findings for all isoforms in 8-h schistosomula were similar to those seen in cercariae prior to exposure (see Fig. 2) and 0.5-h schistosomula (see Fig. 1) in intensity and distribution (representative results for TGF-β_1 are shown in Fig. 3a). For 24 h schistosomula that migrated to the deeper part of the skin, less immunoreactivity in the tegument was found (data not shown). In 48-h schistosomula (Fig. 3b–d), the immunoreactivity in the tegument became almost negative or very faint at the surface. Thus, the expression of TGF-β-like molecules significantly decreased during the skin migrating stage.

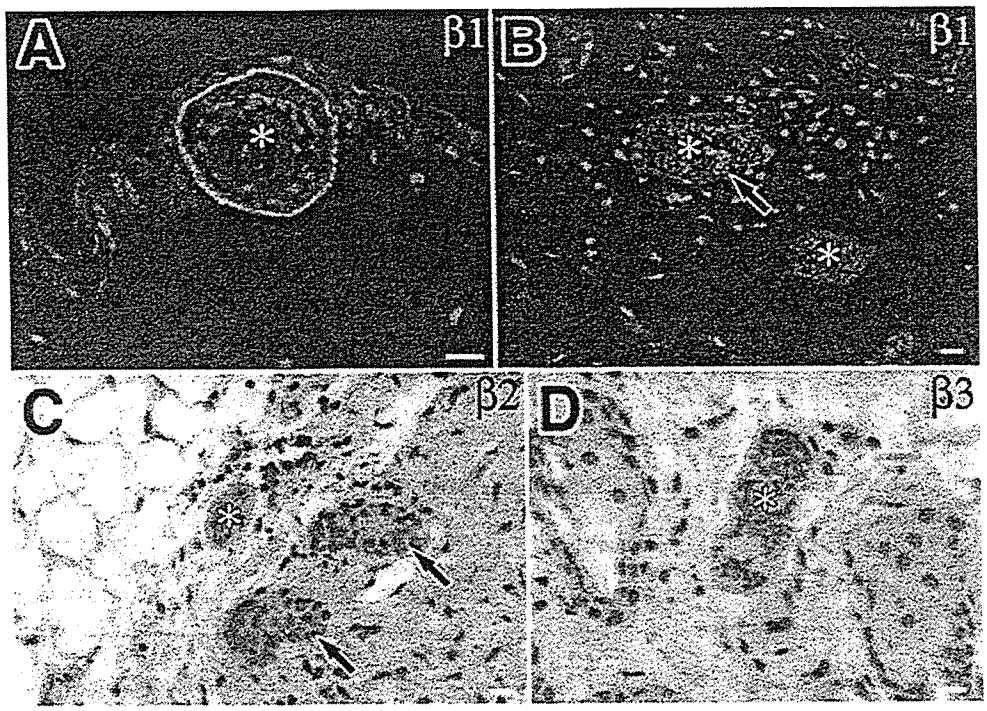

Fig. 3 Changes in TGF-β expression during the skin migrating stage of *S. japonicum* schistosomula. Expression of TGF-β in 8-h (**a**) and 48-h (**b–d**) schistosomula is shown. **a**, **b** Immunofluorescent staining; **c**, **d** immunoenzyme staining. At 8 h the expression of TGF-β_1 in the tegument was still strong (**a**), but had become faint at 48 h (**b**). Expression of TGF-β_2 (**c**) and TGF-β_3 (**d**) took a similar course and disappeared at 48 h. *Asterisks* indicate schistosomula. Note that strong immunoreactivity of TGF-β_1 in the presumed ventral sucker (*arrow* in **b**) remained at 48 h. Weak immunoreactivity for TGF-β_2 was seen in the appendages of the mouse skin (*arrows* in **c**). *Bar* 10 μm

Immunoreactivity in adult worms and eggs

In adult worms, TGF-β_3 immunoreactivity was apparent in subtegumental cells and the lining of gut epithelial cells of males and females (Fig. 4a). Following the peptide blocking test (Fig. 4b), fluorescence completely diminished in the subtegumental cells, but remained in the lining of gut epithelial cells, indicating that only the subtegumental cells were specifically stained. Although other TGF-β isoforms were examined, consistent results were only obtained in TGF-β_3.

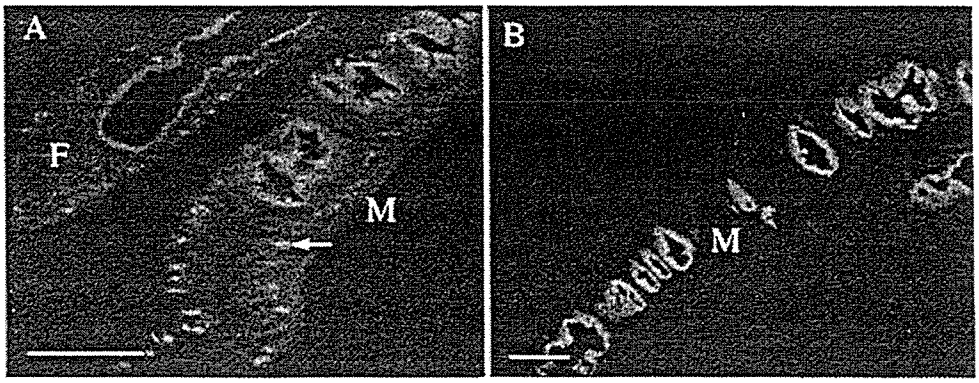

Fig. 4 Immunoreactivity of TGF-β_3 in adult worms. Prior to staining, the primary antibody was incubated with: **a** phosphate-buffered saline or **b** with the corresponding blocking peptide. Subtegumental cells (**a**, *arrow*) were considered as specific, since the reactivity disappeared in the blocking test (**b**). Homogeneous fluorescence in the gut epithelium was unchanged (**b**). *M* Male, *F* female. *Bar* 100 μm

Eggs deposited in the liver also showed strong immunoreactivity for TGF-β_2 on epithelial cells of a tubular-like structure of the miracidial larva (Fig. 5). The positively-stained tissue appeared to be a penetration gland and the associated duct. Other TGF-β isoforms did not yield any consistent results.

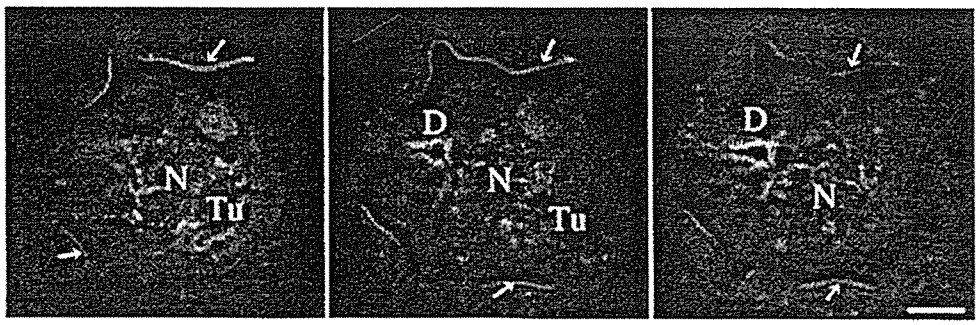

Fig. 5 Localization of TGF-β_1 in a *S. japonicum* egg deposited in mouse liver. Three images of the Z-series reveal TGF-β_2 immunoreactivity in cells of a tubular structure (*Tu*), which was regarded as one of the penetration glands, as well as in the associated duct (*D*). The neural mass (*N*) at the center was considered as negative. *Arrows* indicate eggshell. *Bar* 10 μm

Western blot analysis

In the western blot analysis of cercaria, egg and adult worm extracts, anti-TGF-β antibodies reacted with some molecules under reducing conditions, but differed from the consensus on the mature size of TGF-β (12.5 kDa) (data not shown), suggesting that the immunoreactive molecules found

in this study differ from generally-recognized TGF-β subfamily members with regard to molecular size.

Discussion

We report for the first time the presence of TGF-β-like-immunoreactive molecules throughout the *S. japonicum* life cycle (eggs, cercariae, schistosomula and adult worms). The most prominent expression of TGF-β-like molecules was detected in the tegument covering the whole body of cercariae at the larval stage. CLSM revealed that the molecules may possibly be produced in subtegumental cells and carried to the tegument, as was more evident for TGF-β_3 than the two other isoforms. Consistent expression in the tegument of the body and even the tail seems to reflect a flowing of the surface structure. In addition, the expression in cercariae prior to their penetration into the skin excluded the possibility that the molecules are derived from the mouse host. The specificity of each immunoreactive molecule was confirmed in several control experiments. In particular, our finding that inhibition was observed with the use of each corresponding blocking peptide, but not with unrelated peptides, strongly indicated specificity. In western blot analyses of egg, cercaria and adult worm extract, no band of the expected size was detected, and thus there is some difficulty in identifying the molecular basis of the immunoreactive molecules detected. Nevertheless, our study provides substantial evidence that TGF-β-like molecules that share cross-reactive epitopes with vertebrate TGF-βs are present in the parasites.

TGF-β-like molecules were expressed during the whole life cycle of the parasite, and significant differences were found in the distribution, producing cells and extent of expression with each isoform. In cercariae, TGF-β_2-, and -β_3-immunoreactive cells were greater in number and more widely distributed over the parasite body, whereas TGF-β_1-immunoreactive cells were very few and only a part of the cell body showed reactivity (Fig. 2A). TGF-β_3 and $-\beta_2$ were the predominant isoforms in adult worms and eggs, respectively, although the expression of other isoforms cannot be excluded. These different expression patterns invoke distinct roles for these isoforms during development.

Free-swimming cercariae markedly change their structure and their metabolic activity during transformation from cercaria to schistosomulum to protect themselves against osmotic changes and immune attack from host factors. Studies have shown that within 3 h of skin penetration, the glycocalyx coating of cercaria surface disappears and the trilaminate structure of cercariae, supplied from membranous elements of the subtegumental cells, changes to hepta- or more multi-laminate

and is continuously renewed, which is known to be an essential process for the development of the parasite (Hockley 1973; Sobhon and Upatham 1990). The TGF-β-like molecules identified in our study were localized in the tegument and appeared to be supplied from underlying cells, suggesting that the molecules appear to be one of the tegumental constituents. They continued to be expressed in 8-h schistosomula and then gradually decreased and became almost negative 48 h after skin penetration. This process differed temporally from the dynamic process of the tegumental structure or glycocalyx. Thus, the expression of these molecules appeared to be regulated differently from that of known surface structures. In contrast to the situation in cercariae or schistosomula, the reactive molecules in adult worms were not found in the tegument and there were no indications of transfer from subtegumental cells. In eggs, the molecules were expressed in cells of a tubular structure, suggesting that the molecule is secretory in nature. On the whole, the immunoreactive molecules appear to be involved in distinct roles at each developmental stage.

Here we have shown substantial evidence of TGF-β-immunoreactive molecule expression in most stages of *S. japonicum*, and their stage-specificity suggests a close association with their developmental process. In other studies on parasites, the existence of host cytokine-like molecules, such as homologs of migration inhibition factor in *Burgia malayi* (Pastrana et al. 1998; Pennock et al. 1998), IFN-γ-like protein in *Trichuris muris* (Grencis and Entwistle 1997) and IL-4-like molecules in *Anisakis simplex* (Cuellar et al. 2001) have been reported. In western blot analysis, however, we could not find generally recognized sizes of molecules. In addition, recent analysis of transcriptomes in *S. japonicum* (Hu et al. 2003) and *S. mansoni* (Verjovski-Almeida et al. 2003) has failed to detect conventional TGF-β molecules, suggesting that the molecules differ from conventional ones at least. In another set of experiments which examined TGF-β-like function in schistosome extracts using the Mv1Lu cell proliferation inhibition assay, we found strong inhibitory activity in soluble egg extract and moderate inhibition in worm extract. However, possible contamination of host derived substances or of protease activity in the extracts could not be excluded in the study. Further intensive studies are required to identify the genetic loci and clarify how the TGF-β-like molecules are involved in parasite development.

Acknowledgements The authors thank Ms. Manami Ohba (Department of Parasitology, Kurume University) for her excellent technical assistance. We also express thanks to Mr. Takaaki Kanemaru (Morphology Core, Graduate School of Medical Science, Kyushu University) for his help in preparing photomicrographs, to Mr. Tomokazu Tsutsumi for expert technical assistance and to Dr. Takeshi Nara (Department of Molecular Cell Parasitology, Juntendo University School of

Medicine) for his kind gift of the *S. japonicum* cDNA library. The experimental protocol was approved by the Ethics Review Committee for Animal Experimentation of Kurume University School of Medicine.

References

Beall MJ, Pearce EJ (2001) Human transforming growth factor-beta activates a receptor serine/threonine kinase from the intravascular parasite *Schistosoma mansoni*. J Biol Chem 276:31613–31619

Beall MJ, McGonigle S, Pearce EJ (2000) Functional conservation of *Schistosoma mansoni* Smads in TGF-beta signaling. Mol Biochem Parasitol 111:131–142

Cobbold S, Waldmann, H (1998) Infectious tolerance. Curr Opin Immunol 10:518–524

Cuellar C, Perteguer MJ, Rodero M (2001) Presence of IL-4-like molecules in larval excretory-secretory products and crude extracts from *Anisakis simplex*. Scand J Immunol 53:438–488

Davies SJ, Shoemaker CB, Pearce EJ (1998) A divergent member of the transforming growth factor β receptor family from *Schistosoma mansoni* is expressed on the parasite surface membrane. J Biol Chem 273:11234–11240

Gomez-Escobar N, Van den Biggelaar A, Maizels RM (1997) A member of the TGF-β receptor gene family in the parasitic nematode *Brugia*. Gene 199:101–109

Gomez-Escobar N, Lewis E, Maizels RM (1998) A novel member of the transforming growth factor-β (TGF-β) superfamily from the filarial nematodes *Brugia malayi* and *B. pahangi*. Exp Parasitol 88:200–209

Gomez-Escobar N, Gregory WF, Maizels RM (2000) Identification of tgh-2, a filarial nematode homolog of *Caenorhabditis elegans* daf-7 and human transforming growth factor β, expressed in microfilarial and adult stages of *Brugia malayi*. Infect Immun 68:6402–6410

Grencis RK, Entwistle GM (1997) Production of interferon-gamma homologue by an intestinal nematode: functionally significant or interesting artifact. Parasitology 115:S101-S105

Hirata M, Kage M, Hara T, Nakao M, Fukuma T (1997) Inhibitory effect of circulating egg antigens on *Schistosoma japonicum* egg-induced granuloma formation. J Parasitol 83:842–847

Hirata K, He J, Kuraoka A, Omata Y, Hirata M, Shariful Islam ATM, Noguchi M, Kawabuchi M (2000) Heme oxygenase 1 (HSP-32) is induced in myelin-phagocytosing Schwann cells of injured rat sciatic nerves. Eur J Neurosci 12:4147–4152

Hirata K, He J, Hirakawa Y, Liu W, Wang S, Kawabuchi M (2003) HSP27 is markedly induced in Schwann cell columns and associated regenerating axons. Glia 42:1–11

Hu W, Yan Q, Shen DK, Liu F, Zhu ZD, Song HD, Xu XR, Wang ZJ, Rong YP, Zeng LC, Wu J, Zhang X, Wang JJ, Xu XN, Wang SY, Fu G, Zhang XL, Wang ZQ, Brindley PJ, McManus DP, Xue CL, Feng Z, Chen Z, Han ZG (2003) Evolutionary and biomedical implications of a *Schistosoma japonicum* complementary DNA resource. Nat Genet 35:139–147

Hockley DJ (1973) Ultrastructure of the tegument of *Schistosoma*. Adv Parasitol 11:233–305

Kingsley DM (1994) The TGF-β superfamily: new members, new receptors, and new genetic tests of function in different organisms. Genes Dev 8:133–146

Laemmli UK (1970) Cleavage of structural proteins during the assembly of the head of bacteriophage T4. Nature 227:680–685

Letterio JJ, Roberts AB (1998) Regulation of immune responses by TGF-β. Annu Rev Immunol 16:137–161

Mola PI, Farah OW, Kariuki TM, Nyindo M, Blanton RE, King CL (1999) Cytokine control of the granulomatous response in *Schistosoma mansoni*-infected baboons: role of exposure and treatment. Infect Immun 67:6565–6571

Omer FM, Kurtzhals JA, Riley EM (2000) Maintaining the immunological balance in parasitic infections: a role for TGF-beta? Parasitol Today 16:18–23

Oswald IP, Gazzinelli RT, Sher A, James SL (1992) IL-10 synergizes with IL-4 and transforming growth factor-beta to inhibit macrophage cytotoxic activity. J Immunol 148:3578–3582

Pastrana DV, Raghavan N, Fitzgerald P, Eisinger SW, Metz C, Bucala R, Schleimer RP, Bickel C, Scott AL (1998) Filarial nematode parasites secrete a homologue of the human cytokine macrophage migration inhibitory factor. Infect Immun 66:5955–5963

Pennock JL, Behnke JM, Bickle QD, Devaney E, Grencis RK, Isaac RE, Joshua GW, Selkirk ME, Zhang Y, Meyer DJ (1998) Rapid purification and characterization of L-dopachrome-methylester tautomerase (macrophage-migration-inhibitory factor) from *Trichinella spiralis*, *Trichuris muris* and *Brugia pahangi*. Biochem J 335:495–498

Riddle DL, Albert PS (1997) Genetic and environmental regulation of dauer larva development. In: Riddle DL, Blumenthal T, Meyer BJ, Priess JR (eds) *C. elegans* II. Cold Spring Harbor Laboratory Press, New York, pp 739–768

Takahashi S (1928) On the cercariae of *Schistosoma japonicum*. Katsurada. Okayama Med J 40:1349–1382

Sobhon P, Upatham ES (1990) Snail hosts, life-cycle, and tegumental structure of oriental schistosomes. World Health Organization, Geneva

Verjovski-Almeida S, DeMarco R, Martins EA, Guimarae PE, Ojopi EP, Paquola AC, Piazza JP, Nishiyama MYJr, Kitajima JP, Adamson RE, Ashton PD, Bonaldo MF, Coulson PS, Dillon GP, Farias LP, Gregorio SP, Ho PL, Leite RA, Malaquias LC, Marques RC, Miyasato PA, Nascimento AL, Ohlweiler FP, Reis EM, Ribeiro MA, Sa RG, Stukart GC, Soares MB, Gargioni C, Kawano T, Rodrigues V, Madeira AM, Wilson RA, Menck CF, Setubal JC, Leite LC, Dias-Neto E (2003) Transcriptome analysis of the acoelomate human parasite *Schistosoma mansoni*. Nat Genet 35:148–157

Wahl SM, Frazier-Jessen M, Jin WW, Kopp JB, Sher A, Cheever AW (1997) Cytokine regulation of schistosome-induced granuloma and fibrosis. Kidney Int 51:1370–1375

Williams ME, Caspar P, Oswald I, Sharma HK, Pankewycz O, Sher A, James SL (1995) Vaccination routes that fail to elicit protective immunity against *Schistosoma mansoni* induce the production of TGF-β, which down-regulates macrophage antiparasitic activity. J Immunol 154:4963–4700

Arch Histol Cytol, 68 (1): 29-40 (2005)

The occurrence of nitric oxide synthase-containing axonal baskets surrounding large neurons in rat dorsal root ganglia after sciatic nerve ligation

Wenting Liu, Kazuho Hirata, and Masaru Kawabuchi

Department of Anatomy and Cell Biology, Graduate School of Medical Sciences, Kyushu University, Fukuoka, Japan

Summary. To clarify the possible role of nitric oxide (NO) induced in primary sensory neurons after peripheral axotomy, NO synthase (NOS) immunohistochemistry was carried out on rat L5 dorsal root ganglia after sciatic nerve ligation. The results were compared with the expression of 27-kDa heat shock protein (HSP27), a neuroprotective molecule. In intact animals, NOS-immunoreactive neurons represented about 2% of all dorsal root ganglion (DRG) neurons, whereas HSP27-immunoreactive neurons comprised about 14%. After sciatic nerve ligation, both neurons increased, in number and immunoreactivity, reaching a maximum at 2 weeks, when NOS- and HSP27-immunoreactive neurons represented about 33 and 66%, respectively. NOS-immunoreactive neurons then remained unchanged until 7 weeks although HSP27-immunoreactive neurons showed a slight decline. The increased NOS-immunoreactive neurons were preferentially small (100–500 μm^2) and coexpressed with HSP27 (about 87%). On the other hand, in the proximal stump of sciatic nerves, numerous NOS-immunoreactive fibers with a regenerative profile appeared transiently (2–4 weeks). At higher magnification, an axonal sprout from the NOS-immunoreactive small DRG neurons was found to form a basket-like structure (or basket) mostly around the cell body of NOS-negative large neurons. Retrograde labeling with a fluorescent tracer showed that both neurons sent peripheral axon collaterals to the sciatic nerve. The appearance of this unique structure was most prominent after depletion of the NOS-immunoreactive regenerating fibers in the sciatic nerve (at 7–9 weeks). The findings suggest that NO might be involved in not only axonal regeneration but also the rewiring of two classes of DRG neurons after peripheral nerve injury.

Received October 18, 2004

Address for correspondence: Dr. Kazuho Hirata, Department of Anatomy and Cell Biology, Graduate School of Medical Sciences, Kyushu University, Maidashi 3-1-1, Higashi-ku, Fukuoka, 812-8582 Japan
Tel: +81-92-642-6049, Fax: +81-92-642-6050
E-mail: hirata@anat1.med.kyushu-u.ac.jp

Introduction

Nitric oxide (NO) is an unstable gas that diffuses easily across membranes. It is synthesized from an essential amino acid, L-arginine, by the enzyme NO synthase (NOS) (Bredt and Snyder, 1990), which consists of three different isoforms—the neuronal isoform of NOS (nNOS) in neurons, inducible NOS in macrophages and endothelial NOS in endothelial cells, each being produced by three different genes (for a review see Krumenacker *et al.*, 2004). NO-producing cells are commonly identified by examining the expression of NOS. NOS immunohistochemistry (Zhang *et al.*, 1993; Gonzalez-Hernandez and Rustioni, 1999; Luo *et al.*, 1999; Thippeswamy *et al.*, 2001; Cizkova *et al.*, 2002) and nicotinamide adenine dinucleotide phosphate diaphorase (NADPHd) histochemistry (Fiallos-Estrada *et al.*, 1993), an established method for NOS detection, have shown that nNOS is constitutively expressed in some adult dorsal root ganglion (DRG) neurons, and peripheral axotomy results in a significant increase in NOS-containing neurons in the dorsal root ganglia (DRGs). This finding is consistent with those of in situ hybridization (Verge *et al.*, 1992), RNase protection assays (Luo *et al.*, 1999), and NOS radioassay (Cizkova *et al.*, 2002). As for the role of induced NO in the DRGs after peripheral axotomy, the predominant view is that it has a neuroprotective action

preventing the loss of neurons and facilitating regeneration (Gonzalez-Hernandez and Rustioni, 1999; for a review see Thippeswamy and Morris, 2002). On the other hand, NO is multifunctional (for reviews see Iadicola, 1997 and Krumenacker *et al.*, 2004) and might therefore play other roles: as a neuronal messenger involved in nociceptive transmission (Meller *et al.*, 1992; Choi *et al.*, 1996; Cizkova *et al.*, 2002), and a neurotoxin as reported in avulsed motor neurons (Wu and Li, 1993; Wu *et al.*, 1994; Novikov *et al.*, 1995; Estevez *et al.*, 1998). Thus, the role of the induced NO in axotomized DRG neurons requires further clarification.

The 27-kDa heat shock protein (HSP27) is induced in cells of many types of tissues by stressful stimuli and plays important roles in cellular repair and protective mechanisms (for a review see Ciocca *et al.*, 1993). This protein is reportedly overexpressed in the nervous system under simulated pathological conditions (Kato *et al.*, 1994, 1995; Plumier *et al.*, 1996; Imura *et al.*, 1999; He *et al.*, 2003; Hirata *et al.*, 2003) as well as with serious brain diseases such as Alexander's disease (Iwaki *et al.*, 1993), Alzheimer's disease (Shinohara *et al.*, 1993), and Parkinson's disease (Renkawek *et al.*, 1994). Costigan *et al.* (1998) reported that HSP27 in adult rat DRGs was upregulated after transection of the sciatic nerve—although their study did not focus on changes in HSP27 expression with time. From this finding and the results of their subsequent experiments on neonatal neuronal survival after axotomy *in vivo* and after nerve growth factor (NGF) withdrawal in vitro (Lewis *et al.*, 1999), they concluded that this protein might contribute to cytoskeleton alterations associated with axonal growth and promote the survival of injured sensory neurons. Thus, HSP27 plays a role in neuroprotection in injured or stressed primary sensory neurons and is accordingly a possible marker for these neurons.

To explore the role of NO in injured DRG neurons, the present study immunohistochemically examined alterations of NOS expression in DRGs and the sciatic nerve after ligation, and compared the results with HSP27 expression in DRG neurons. Our data showed a prominent increase in NOS-immunoreactive small DRG neurons, most of which were positive for HSP27, after nerve ligation. The small neurons remained there, even after depletion of the NOS-immunoreactive regenerating fibers in the sciatic nerve, and extended the axonal sprouts which formed a basket-like structure around an NOS-negative large neuron. Further experiments with a retrograde tracer revealed that both of the neurons were axotomized. In addition, the role of *de novo* induced NO in primary sensory neurons was considered.

Materials and Methods

Surgery

Twenty-five adult Wistar rats of both sexes, weighing 180–200 g and aged 6 to 8 weeks, were used for all experiments. After being anesthetized with sodium pentobarbital (50 mg/kg), the proximal one-third of the right sciatic nerve was exposed and tightly ligated with 4-0 silk sutures. The rats were kept alive for 2 and 7 days, and 2, 4, 7 (n=4 at each time point), and 9 weeks (n=3). Two unoperated rats were used as controls.

NOS and HSP27 immunohistochemistry

All animals except those kept alive 9 weeks were deeply anesthetized and transcardially perfused with phosphate buffer saline (PBS) followed by 4% paraformaldehyde in a 0.1 M phosphate buffer (PB), pH 7.4. The L5 DRGs and sciatic nerves on both the operated and unoperated sides were removed and postfixed for 4 h in the same fixative used for perfusion. All materials were put in 30% sucrose in PB for cryoprotection overnight at 4℃, after which 20 μm thick serial sections were cut with a cryostat. The DRG sections were grouped into four parallel series: the first for green fluorescent Nissl staining, the second for single immunofluorescent labeling of HSP27 and fluorescent Nissl staining, the third for double immunofluorescent labeling of HSP27 and NOS, and the fourth for single

Fig. 1. Expression of NOS in longitudinal sections of an intact sciatic nerve used as a control (**A**) and sciatic nerves at 2 days (**B**), 2 weeks (**C**), 4 weeks (**D**) and 7 weeks (**E**) after tight ligation, and enlarged images of the proximal stump at 4 weeks (**F**). NOS-immunoreactive fibers are hardly seen in the intact nerve (**A**), whereas after ligation, a small number appeared in the proximal stump at 2 days (**B**), increasing at 2 (**C**) and 4 weeks (**D**) and then decreasing at 7 weeks (**E**). Note the NOS-immunoreactive fibers extending towards the distal stump alongside the ligature (which shows intense autofluorescence indicated by an asterisk in **D**) at 4 weeks. Higher magnification of the NOS-immunoreactive fibers seen in the proximal stump at 4 weeks shows varicosities and swelling in some regions running retrogradely, suggesting a regenerating profile (**F**). Asterisks in **B**, **C** and **E** show the ligation site. Scale bars=100 μm (A–E), 10 μm (F)

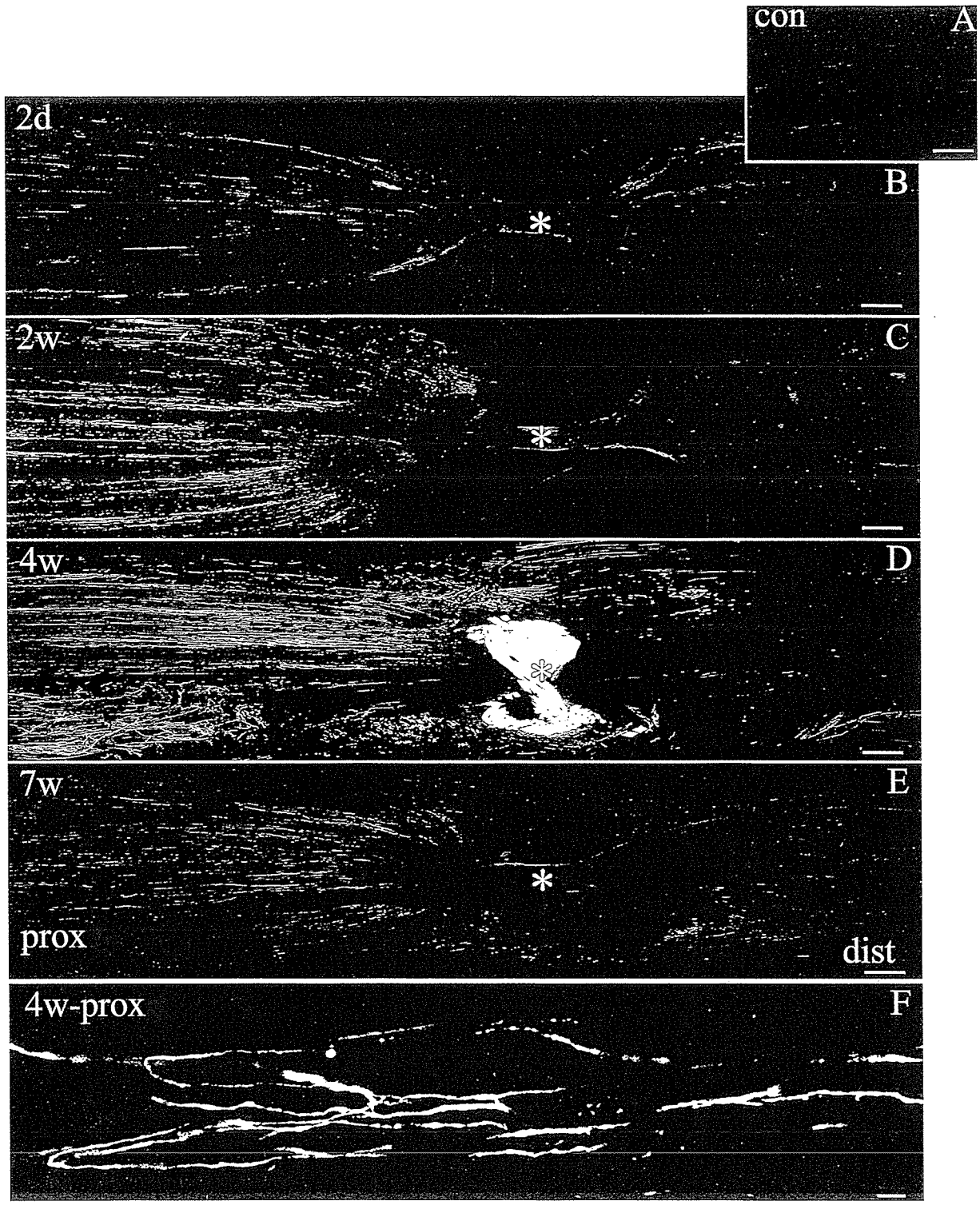

Fig. 1. Legend on the opposite page.

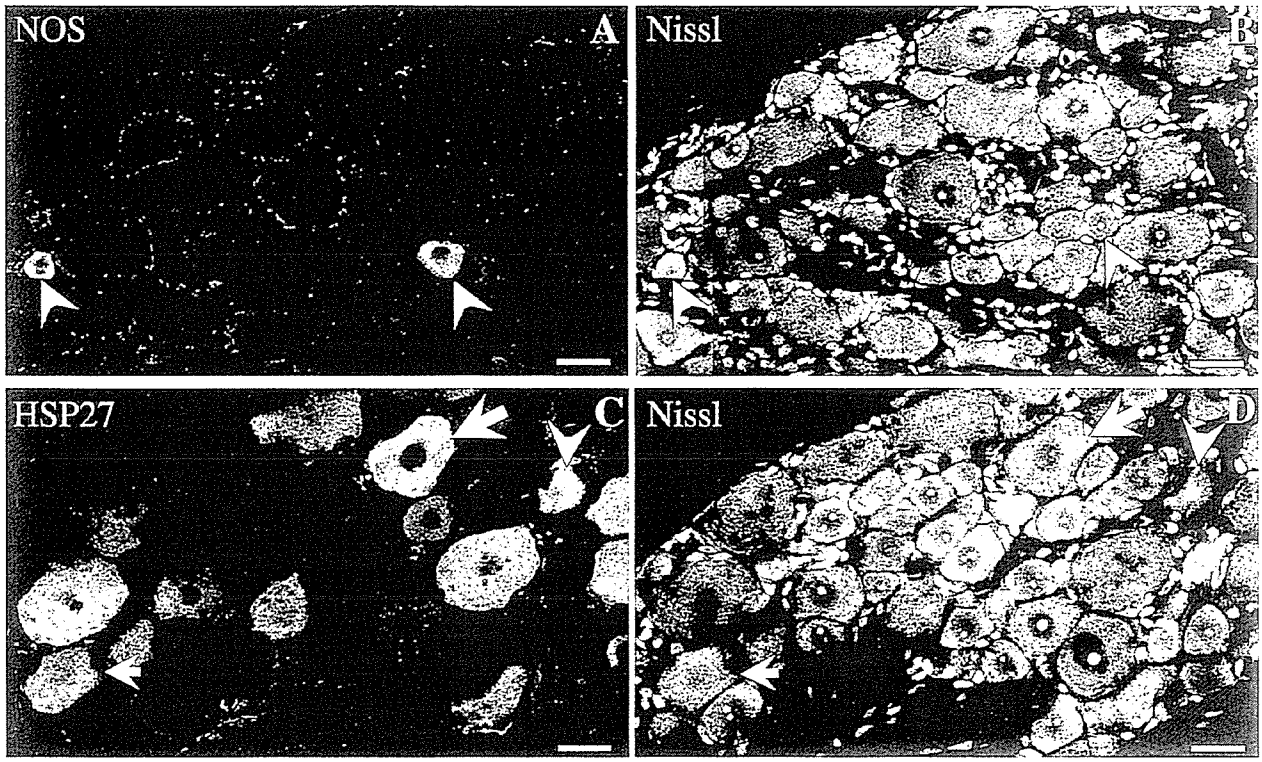

Fig. 2. A NOS immunofluorescent-labeled (**A**) and fluorescent Nissl-stained (**B**) section and an HSP27 immunofluorescent-labeled (**C**) and fluorescent Nissl-stained (**D**) section of L5 DRG from an intact animal. Arrowheads indicate small neurons, and the small or large arrow shows a medium or large neuron, respectively. Scale bars=30 μm

immunofluorescent labeling of NOS and fluorescent Nissl staining. The sciatic nerve sections were only processed for immunofluorescent labeling of NOS.

The immunohistochemical procedures used in the present study has been described in detail in our previous articles (He *et al.*, 2003; Hirata *et al.*, 2003). Briefly, non-specific binding sites were blocked by preincubation with 0.1% bovine serum albumin (BSA) in PBS containing 0.5% Triton X-100 overnight at 4℃. For single immunfluorescent labeling of NOS, the sections were first incubated with sheep polyclonal antibodies (pAb) raised against brain NOS (1:2000; donated by Dr. Emson) and then with biotinylated donkey anti-sheep IgG (Jackson, USA) overnight at room temperature (RT). For visualization of the biotin-binding site, Texas red-streptavidin was used. For single immunofluorescent labeling of HSP27, rabbit pAb raised against murine HSP25 which specifically recognized rat HSP27 (Head *et al.*, 1994; Plumier *et al.*, 1996) (StressGen, SPA-801) was used. The sections were first incubated with rabbit pAb to HSP25/27 diluted in PBS (1:1500) for 36 h at RT and then with Texas red-conjugated donkey anti-rabbit IgG (Jackson) overnight at RT. Control sections were processed in the same way and in parallel, except that they were incubated with PBS instead of primary antibodies. No stained structures were observed in the controls. The sections Texas red-labeled for NOS or HSP27 were counter-stained with green fluorescent Nissl-stain solution (NeuroTrace 500/525 green fluorescent Nissl-stain, N-21480, Molecular Probes) for quantifying the total number of DRG neurons (cf. Fig. 2A, B, C, D).

For double immunofluorescent labeling of HSP27 and NOS, a mixture of rabbit pAb to HSP25/27 and sheep pAb to NOS was used as the primary antibody. Then a mixture of Texas red-conjugated donkey anti-rabbit IgG (Jackson) and Alexa488-conjugated donkey anti-goat IgG (Molecular Probes) was used as the secondary antibody. No differences in the morphology of any of the immunolabeled structures were noted between the single and double labeled samples.

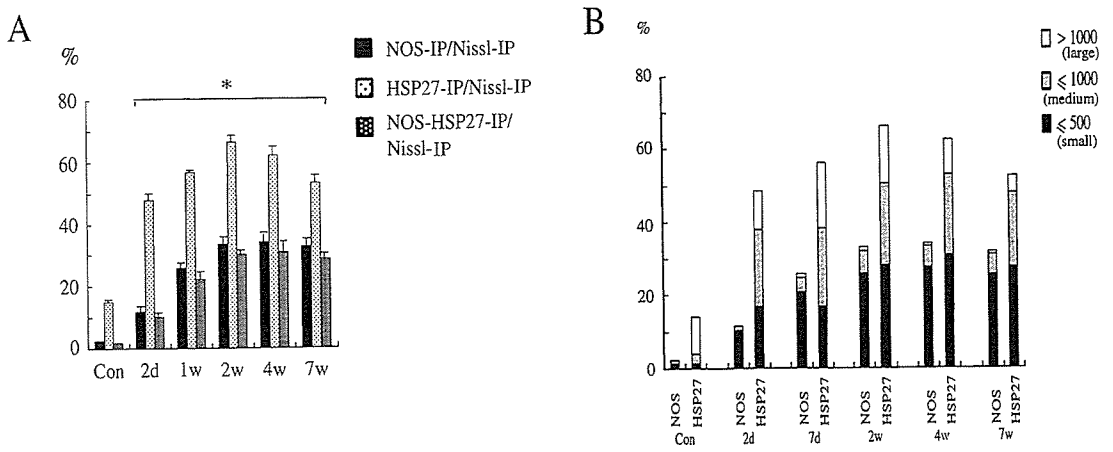

Fig. 3. A: Changes in the number of NOS-, HSP27-immunoreactive and NOS- and HSP27-double-immunoreactive neurons in the L5 DRGs following sciatic nerve ligation. Three animals were used at each time point. Data are the mean ± S.D. (bars). Values of NOS- and HSP27-immunoreactive neurons are expressed as percentages compared with the total number of fluorescent Nissl-stained DRG neurons in each of the same sections, and that of NOS- and HSP27-double-immunoreactive neurons have been compared with the average of the total number. * $p<0.05$. **B:** Changes in neuronal size in NOS- and HSP27-immunoreactive DRG neurons following sciatic nerve ligation. Three animals were used at each time point. Note that a gradual increase and subsequent persistent occurrence of NOS-immunoreactive small neurons occur after nerve ligation, paralleling the occurrence of HSP27-immunoreactive small neurons.

Retrograde tracing with a fluorescent dye

To examine whether NOS-immunoreactive small DRG neurons forming a pericellular basket were axotomized, three animals received an application of a retrograde fluorescent tracer, dextran fluorescein (FITC) (3000 MW, anionic lysine fixable, Molecular Probes) at 9 weeks after ligation. The ligated sciatic nerve was cut at a point 1 mm proximal from the ligation site, and the proximal stump was placed in 2 μl of 4% saline-dissolved dextran FITC in a small plastic tube with a blinded end. The nerve was then glue-packed in the tube to prevent any leakage of the tracer. Two or three days after tracer injection, the animals were perfused with the same fixative and the DRGs were removed (Kobayashi *et al.*, 2003). The sections were processed for NOS immunohistochemistry and labeled with Texas red.

Confocal laser scanning microscopy

The sections double-labeled with one of the green fluorescent dyes (Nissl, Alexa 488, or FITC) and Texas red were scanned using excitation at 488 nm (argon laser) for the former and at 568 nm (krypton laser) for the latter by confocal laser scanning microscopy (CLMS; LSM-GB200, Olympus, Japan). Images were scanned using a 10 × objective lens. To avoid cross-talk, separate single optical sections were scanned for each fluorescence (channels 1 and 2) and then superimposed. For the pericellular baskets, images were taken using a 40 × objective lens, and serial optical sections were projected at intervals of 1.2 μm and extended on a single plane with a thickness of 12 to 14 μm (volume projection method).

Counting of neurons and pericellular baskets

Changes in the number of the immunoreactive neurons at each time point were analyzed by using the NIH image program. In every fourth section, the total numbers of HSP27- and NOS-immunoreactive, or HSP27- and NOS-double-immunoreactive neurons with a clearly visible nucleus, were separately counted. The ratio of NOS- or HSP27-immunoreactive neurons was expressed as a percentage to the total number of fluorescent Nissl-stained DRG neurons in the same section . The ratio of NOS- and

HSP27-double-immunoreactive neurons was expressed as a percentage to the average total number of fluorescent Nissl-stained neurons in the next two sections. The total number of fluorescent Nissl-stained neurons showed no significant difference among DRGs from ipsilateral and contralateral sides, and intact animals. Two forms of Student's t-test were utilized to compare the means of each parameter. To increase the reliability of measured data, Student's t-test was applied between DRGs from the ipsilateral sides and controls. The difference between the two values was considered significant if the probability value (P) was less than 0.05.

The number of pericellular baskets was counted in NOS- and HSP27-double-immunofluorescent labeled sections and NOS-immunofluorescent labeled sections treated with retrograde labeling. A pericellular basket was defined as a NOS-immunoreactive component running closely adjacent to the somatic profile >70 % of its circumference.

Size measurements

Changes in the sizes of the NOS- or HSP27-immunoreactive DRG neurons at each time point were analyzed by tracing the circumferences of the somata using the same image program.

All experiments were reviewed by the Committee on Ethics for Animal Experiments of the Faculty of Medicine, Kyushu University, and carried out according to the University's Guidelines for Animal Experiments and Law No. 105 and Notification No. 6 of the Japanese Government.

Results

NOS immunohistochemistry in sciatic nerves

In the intact sciatic nerves, few NOS-immunoreactive fibers were seen (Fig. 1A), but at 2 days after ligation, a small number of NOS-immunoreactive fibers appeared in the proximal stump near the ligature (Fig. 1B). At 2 weeks, the proximal stump was extremely swollen and numerous NOS-immunoreactive fibers with strong immunoreactivity were seen (Fig. 1C). At 4 weeks, the increased numbers of NOS-immunoreactive fibers were still visible in the proximal stump, but some ran alongside the ligature towards the distal stump (Fig. 1D). At higher magnification, the NOS-immunoreactive fibers in the proximal stump with strong immunoreactivity showed profiles characteristic of regrowing axons, such as varicosities and swelling in the sinuous course as previously reported by Gonzalez-Hernandez and Rustioni (1999), and they often became recurrent (Cajal, 1928) (Fig. 1F). Thereafter, the NOS-immunoreactive fibers gradually decreased and only a small number with less immunoreactivity were detected at 7 weeks (Fig. 1E).

NOS and HSP27 immunohistochemistry in DRGs

In the DRGs of the contralateral side and from intact animals, NOS was weakly expressed in a small number of neurons (approximately 2%) (Fig. 2A, B, 3A, B), whereas HSP27 was expressed in a greater number (about 14%) (Fig. 2C, D, 3A, B) with varying degrees of immunoreactivity (Fig. 4A). The NOS-immunoreactive neurons consisted of small (100-500 μm^2) (Fig. 2A, B) to medium neurons (500−1000 μm^2) (Fig. 3B), whereas HSP27-immunoreactive neurons consisted of a majority of large neurons (>1000 μm^2) with a small proportion of small and medium neurons (Fig. 2C, D, 3B). Double immunofluorescent labeling showed that most of the NOS-immunoreactive neurons were positive for HSP27 (Fig. 3A) although the expression of both proteins was usually weak (Fig. 4A).

After sciatic nerve ligation, the NOS-immunoreactive neurons significantly increased in number (Fig. 3A) and usually showed strong immunoreactivity (Fig. 4B, C, D). At 2 days, NOS-immunoreactive neurons comprised six times the original number in the controls (approximately 12%), then gradually increased and reached a peak at 2 weeks (approximately 33%). Thereafter the NOS-immunoreactive neurons maintained strong immunoreactivity until 7 weeks (Fig. 3A) even though the NOS-immunoreactive fibers within the sciatic nerves decreased at this point (Fig. 1E). Size frequency analysis (Fig. 3B) revealed that the majority of *de novo* NOS-immunoreactive subpopulations at each

Fig. 4. Pseudo-color images of the double immunofluorescent labeling of NOS (green) and HSP27 (red) in the DRG from an intact animal (**A**) and ipsilateral DRGs at 2 days (**B**), 2 weeks (**C**) and 7 weeks (**D**) after sciatic nerve ligation. Only one weakly stained NOS and HSP27-double-immunoreactive small neuron (yellowish green) is seen in the intact DRG (**A**). Intensely stained NOS and HSP27-double-immunoreactive small neurons (bright yellow) appear at 2 days (**B**) and increase at 2 weeks (**C**) after ligation. At 7 weeks (**D**), HSP27 expression becomes weaker in most double-immunoreactive small neurons so that most become yellowish green. Scale bar=100 μm (for A−D)

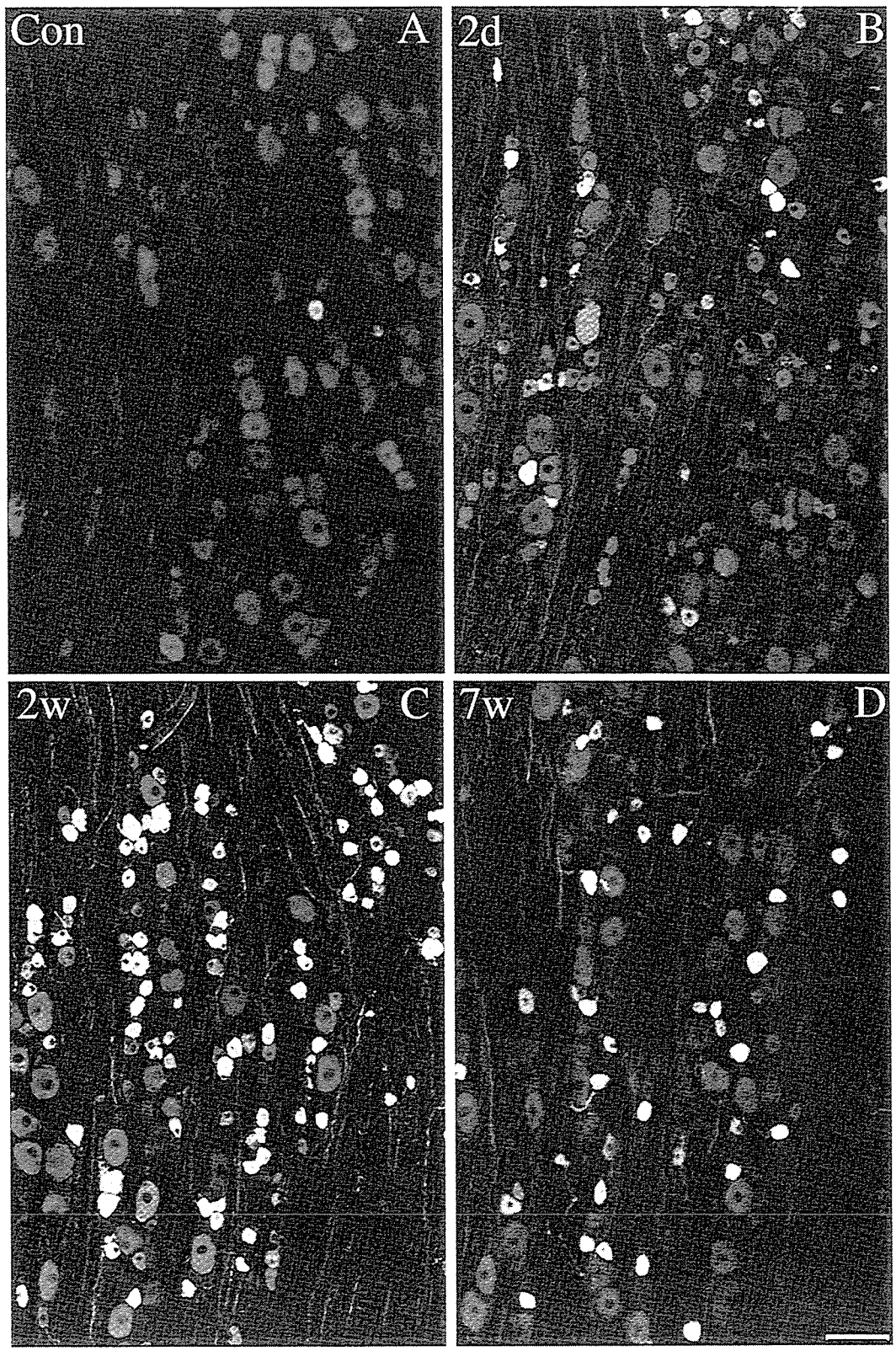

Fig. 4. Legend on the opposite page.

time point after ligation were composed of small neurons.

After nerve ligation, the HSP27-immunoreactive neurons also increased in number (Fig. 3A) and some of them, especially the small neurons, showed stronger immunoreactivity (Fig. 4B, C) than that seen in the controls. At 2 days, HSP27-immunoreactive neurons reached more than three times the original number in the controls (about 48%). This number further increased and reached a peak at 2 weeks (approximately 66%). They then slightly declined, reaching about 53% at 7 weeks (Fig. 3A), with most also reduced in immunoreactivity (Fig. 4D). Thus, the pattern of changes was similar between NOS- and HSP27-immunoreactive neurons until postoperative week 2, but thereafter the latter slightly decreased in number and immunoreactivity while the former remained unchanged. Size frequency analysis (Fig. 3B) showed that, after nerve ligation, the number of HSP27-immunoreactive small and medium neurons markedly increased, whereas that of HSP27-immunoreactive large neurons was only slightly altered. Especially the HSP27-immunoreactive small neurons prominently increased at 2 weeks, representing almost half of all the HSP27-immunoreactive neurons, and then remained unchanged until 7 weeks (Fig. 3B). Double immunofluorescent labeling showed that most NOS-immunoreactive neurons were also positive for HSP27 at each time point (about 87%) (Fig. 3A, 4B, C, D)—although in these neurons the HSP27 immunoreactivity was considerably reduced at 7 weeks (Fig. 4D).

Pericellular baskets formed by NOS-immunoreactive sprouts in DRGs

Observations under higher magnification revealed the formation of basket-like structures after nerve ligation, in which NOS-immunoreactive fibers usually surrounded the cell body of NOS-negative large neurons (Fig. 5A, B, D), and in some cases, that of NOS-immunoreactive small neurons (Fig. 5C). This pericellular basket was hardly visible at 2 weeks although at this time point NOS-immunoreactive fibers appeared in the nerve bundles within the DRGs (Fig. 4C), occurring concurrently with the marked increase in the proximal stump of the sciatic nerves (Fig. 1C). The NOS-immunoreactive baskets were first detected at 5 weeks and thereafter the numbers increased. We counted the number of baskets in every second section at 7 and 9 weeks. At 7 weeks after nerve ligation, the density of NOS-immunoreactive baskets ranged from 0.4 to 3.2/section in the L5 DRG of 3 rats (mean 1.4 ± 0.5, $n=30$ sections). At 9 weeks, it ranged from 2.4 to 3.2/section among 3 rats (mean 2.8 ± 1.3, $n=38$ sections). These findings suggest that the formation of the baskets was ongoing during this period. Double immunofluorescent labeling showed that the NOS-immunoreactive baskets hardly coexpressed with HSP27 (Fig. 5A). No pericellular baskets were detected in DRG sections from intact animals ($n=16$ sections), and only 2 were seen in a few sections from the contralateral side ($n=12$ sections). Thus, most of the baskets seemed to appear as a direct result of peripheral nerve ligation. In some cases the NOS-immunoreactive fibers that formed the baskets could be traced to their origin and were shown to be formed by axonal sprouts from cell bodies of NOS-immunoreactive small neurons lying 1–3 cell diameters away (Fig. 5B, D).

NOS-immunohistochemistry of the DRG receiving a retrograde labeling with a fluorescent tracer, dextran-FITC, revealed that most of the NOS-immunoreactive small neurons became heavily retrograde-labeled (Fig. 5D). NOS negative large neurons surrounded by the NOS-immunoreactive baskets were also often labeled with dextran-FITC although they were usually less intensely labeled compared with small neurons (Fig. 5D). Retrograde labeling was detected in about 82% (82/99) of the neurons associated with NOS-immunoreactive baskets. Consequently, in some cases the axonal sprout from the dextran-labeled NOS-immunoreactive small neurons formed the baskets around the dextran-labeled NOS negative large neurons (Fig. 5D). Thus, these findings suggest the possibility of a rewiring of two classes of axotomized neurons.

Discussion

The present study has clearly shown a significant increase in NOS-immunoreactive DRG neurons after sciatic nerve ligation. This result is basically in accordance with that studied in various experimental models of peripheral nerve injury, such as transection (Fiallos-Estrada *et al.*, 1993; Zhang *et al.*, 1993), resection (Verge *et al.*, 1992; Thippeswamy *et al.*, 2001), loose ligation (Cizkova *et al.*, 2002) and tight ligation (Gonzalez-Hernandez and Rustioni, 1999) of the sciatic nerves, and tight ligation of L5 and L6 spinal nerves (Luo *et al.*, 1999). The increased NOS-immunoreactive DRG neurons were mainly small neurons, as reported in other studies (Gonzalez-Hernandez and Rustioni, 1999; Luo *et al.*, 1999). The number of HSP27-immunoreactive DRG neurons also increased after nerve ligation; these neurons were mainly small and medium sized, as reported Costigan *et al.* (1998).

The present study includes a new finding that the NOS-immunoreactive small neurons were mostly coexpressed with HSP27. Statistical analysis showed that the NOS and HSP27-double-immunoreactive small DRG neurons—

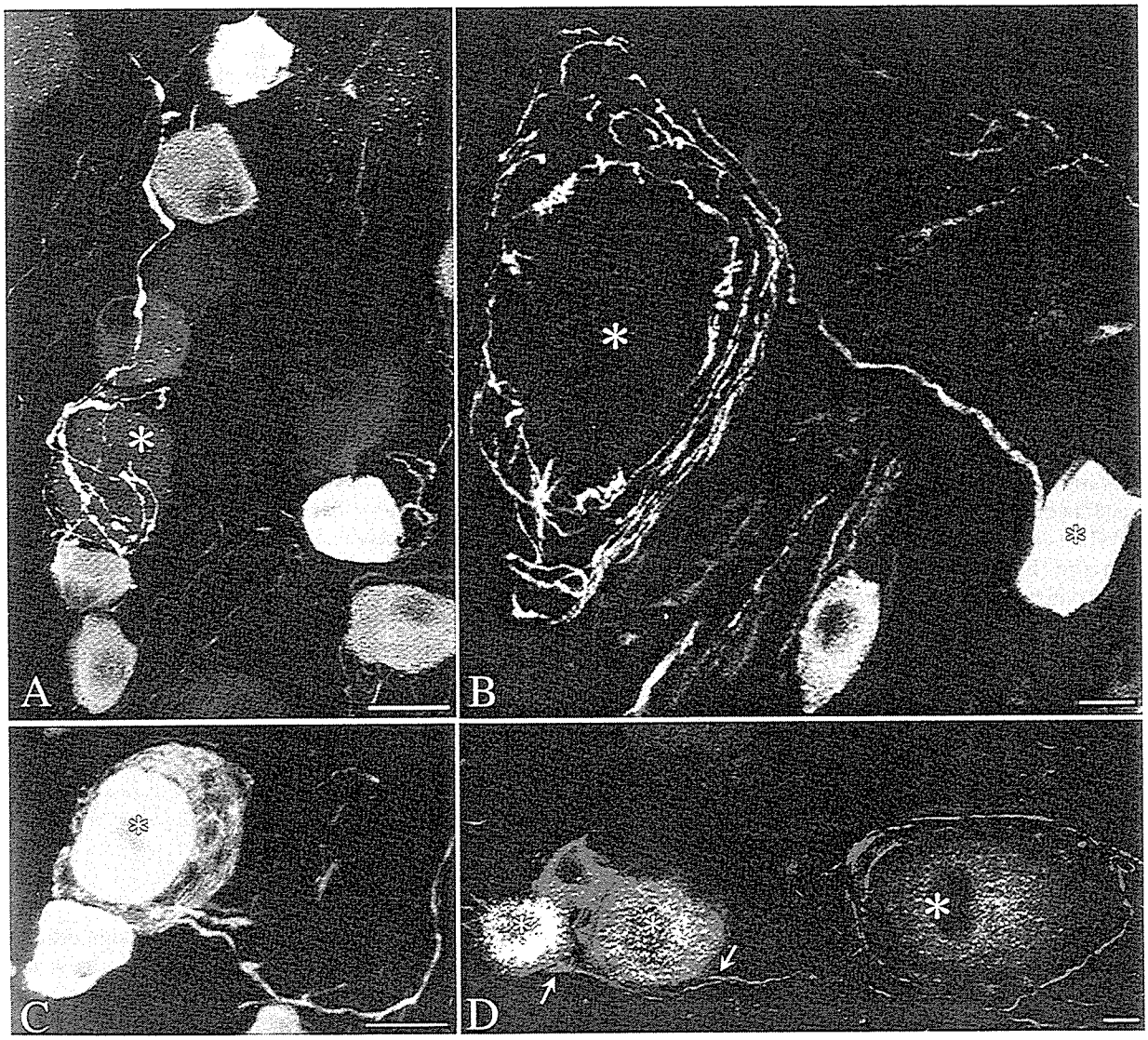

Fig. 5. Pseudo-color images of the NOS-immunoreactive baskets that form around the NOS-negative large neurons (**A**, **B** and **D**) or NOS-immunoreactive small neurons (**C**) from 5 (**A**) and 9 weeks (**B**, **C** and **D**) after sciatic nerve ligation. **A:** Double immunofluorescent labeling of NOS (green) and HSP27 (red) showing a basket consisting of an elaborate NOS-immunoreactive axonal plexus with numerous varicosities surrounding a tangentially sectioned large neuronal profile (the large asterisk). Note that no coexpression with HSP27 in the basket is seen. **B:** NOS immunofluorescent labeling showing a NOS-immunoreactive axonal sprout from a strongly stained NOS-immunoreactive small neuron (the small asterisk) repetitively surrounding a large neuronal profile (a large asterisk) presumably sectioned through the center of the neuron. **C:** NOS immunofluorescent labeling showing a smooth NOS-immunoreactive fiber repetitively surrounding an intensely stained-NOS-immunoreactive small neuron. **D:** Retrograde labeling with FITC-dextran (green or yellow) and NOS immunofluorescent labeling (red) showing that two retrograde-labeled NOS-immunoreactive small neurons (small asterisks) send axonal sprouts (arrows) to form the baskets surrounding a retrograde-labeled NOS negative large neuron (the large asterisk). Scale bars=20 μm (A–C), 10 μm (D)